Neutrino mean free paths in cold symmetric nuclear matter

S. Cowell and V. R. Pandharipande
Department of Physics, University of Illinois at Urbana-Champaign, 1110 W. Green St., Urbana, Illinois 61801, USA
(Received 23 April 2004; published 23 September 2004)

The neutrino mean free paths (NMFP) for scattering and absorption in cold symmetric nuclear matter (SNM) are calculated using two-body effective interactions and one-body effective weak operators obtained from realistic models of nuclear forces using correlated basis theory. The infinite system is modeled in a box with periodic boundary conditions and the one particle-hole (p-h) response functions are calculated using the Tamm-Dancoff approximation (TDA). For the densities $\rho=\frac{1}{2}$, 1, $\frac{3}{2}\rho_0$, where ρ_0 is the equilibrium density of SNM, the strength of the response is shifted to higher energy transfers when compared to a noninteracting Fermi gas (FG). This and the weakness of effective operators compared to the bare operators, significantly reduces the cross sections, enhancing the NMFP by factors of $\sim 2.5-3.5$ at the densities considered. The NMFP at the equilibrium density ρ_0 are also calculated using the TDA and random phase approximation (RPA) using zero range Skyrme-like effective interactions with parameters chosen to reproduce the equation of state and spin-isospin susceptibilities of matter. Their results indicate that RPA corrections to correlated TDA may further increase the NMFP by $\sim 25\%$ to $3-4$ times those in a noninteracting FG. Finally, the sums and the energy weighted sums of the Fermi and Gamow-Teller responses obtained from the correlated ground state are compared with those of the 1 p-h response functions to extract the sum and mean energies of multi p-h contributions to the weak response. The relatively large mean energy of the multi p-h excitations suggests that they may not contribute significantly to low energy NMFP.

DOI: 10.1103/PhysRevC.70.035801 PACS number(s): 21.65.+f, 26.50.+x, 25.30.Pt, 13.15.+g

I. INTRODUCTION

In the past decade it has become clear that neutrinos play a dominant role in many astrophysical processes. In the context of supernovae and neutron stars, for example, it is essential to know neutrino interactions with nuclear matter, while modern neutrino detectors such as KARMEN and MiniBooNE, used to study neutrino properties, require an understanding of neutrino-nucleus interactions. Theoretically, essentially exact neutrino interaction rates can be calculated only in the lightest nuclei [1] where *ab initio* calculations are possible with realistic interactions. In recent years, much effort has been directed to developing more accurate approximation methods to calculate neutrino reaction rates and luminosities. Neutrino interactions with nuclei have been calculated using, for example, shell model and random phase approximation (RPA) [2,3]. While for infinite matter, recent calculations have used mean field or Fermi liquid theories and the RPA [4–7].

For conditions relevant in neutron stars and core collapse supernovae, these earlier calculations have found a significant reduction in reaction rates associated with correlations in the nuclear wave function. For example, using Skyrme-like effective interactions and RPA, Reddy *et al.* [6] obtain an enhancement of the neutrino mean free path (NMFP) of $\sim 2-3$ in hot asymmetric matter. Similar effects on neutrino mean free paths (NMFP) due to scattering of neutrinos by neutral weak currents in hot neutron matter were found by Iwamoto and Pethick [7] using Fermi liquid theory. These calculations have incorporated the effects of correlations in the nuclear wave function through empirical effective interactions or Landau parameters. However, they have neglected the effects of correlations on the operators and used bare weak operators. It is well known that this treatment is inconsistent [8] and that a consistent set of effective operators and effective interactions must be included in a more accurate treatment.

As a first step toward a more consistent treatment of neutrino interactions, a previous article [9], hereafter referred to as I, described a consistent set of effective interactions and effective weak operators developed starting from realistic interactions using correlated basis theory (CBT). The charge current effective operators were found to be quenched by $\sim 20-25\,\%$ relative to the bare operators, indicating that neutrino cross sections predicted by previous calculations using bare weak operators may be overestimated. We present here the next essential step in the ongoing program to predict NMFP in supernovae and neutron star matter. NMFP for scattering and absorption in cold symmetric nuclear matter (SNM) are calculated using the two-body effective interactions and one-body effective weak operators obtained in I.

The structure of the paper is as follows. A brief review of the effective interactions and effective weak operators in CBT is given in Sec. II. The infinite system is modeled in a box with periodic boundary conditions and response functions are calculated using the Tamm-Dancoff approximation (TDA). These methods are discussed in detail in Sec. III. The charge and neutral current response functions are presented in Secs. IV and V, respectively. These are used to determine NMFP for neutrino absorption and scattering in Sec. VI. A comparison of response functions and NMFP obtained using CBT and Skyrme-like effective interactions is presented in Sec. VII. Results of RPA calculations using such Skyrme interactions are given in Sec. VIII. Estimates of the mean energy of neutrino response via multi-particle-hole excitations of matter using response sums and energy weighted sums are discussed in Sec. IX. Conclusions and future projects are discussed in Sec. X.

II. EFFECTIVE INTERACTION AND OPERATOR

In this section we briefly review the two-body effective interaction, v_{ij}^{CB} and one-body effective weak operators, $O_W^{eff(1b)}$, obtained previously using CBT. The reader is referred to I for details.

In CBT the nuclear states are defined as

$$|\Psi_X\rangle = \left(\mathcal{S}\prod_{i<j} F_{ij}\right)|\Phi_X\rangle, \tag{1}$$

where $|\Phi_X\rangle$ are uncorrelated Fermi gas (FG) states and $\mathcal{S}\Pi F_{ij}$ denotes the symmetrized product of pair correlation operators given by

$$F_{ij} = \sum_{p=1,6} f^p(r_{ij}) O_{ij}^p. \tag{2}$$

$$O_{ij}^{p=1,6} = 1, \boldsymbol{\tau}_i \cdot \boldsymbol{\tau}_j, \boldsymbol{\sigma}_i \cdot \boldsymbol{\sigma}_j, \boldsymbol{\tau}_i \cdot \boldsymbol{\tau}_j \boldsymbol{\sigma}_i \cdot \boldsymbol{\sigma}_j, S_{ij}, \boldsymbol{\tau}_i \cdot \boldsymbol{\tau}_j S_{ij}. \tag{3}$$

The pair correlation functions, $f^p(r_{ij})$, are obtained by minimizing the energy of SNM using Fermi hypernetted and single operator chain summation methods (FHNC-SOC) [10,11]. These variational calculations also include spin-orbit correlations, which are neglected in the present work. The correlated states $|\Psi_X\rangle$ are not necessarily orthogonal. They can be orthonormalized as discussed in Ref. [12]. However, in I and here we have neglected the orthogonality corrections. They should be included, together with many-body cluster contributions, in a more accurate treatment.

The FG states $|\Phi_X\rangle$ are specified by the occupation numbers $n_X(\mathbf{k}, \sigma, \tau)$ of plane wave single particle states with momentum $\mathbf{k}$ and spin-isospin σ, τ, in the many-body state X. The FG ground state $|\Phi_0\rangle$ of SNM has $n_0(\mathbf{k}, \sigma, \tau) = \Theta(k_F - |k|)$, where k_F is the Fermi momentum. It is often convenient to specify the FG states by particle-hole excitations of the ground state. For example,

$$|\Phi_{1p,1h}\rangle = a^\dagger_{\mathbf{p},\sigma_p,\tau_p} a_{\mathbf{h},\sigma_h,\tau_h} |\Phi_0\rangle. \tag{4}$$

The correlated states $|\Psi_X\rangle$ are in one-to-one correspondence with the FG states via Eq. (1). Thus they can also be labeled with particle-hole excitations of the correlated ground state:

$$|\Psi_{1p,1h}\rangle = \left(\mathcal{S}\prod_{i<j} F_{ij}\right)|\Phi_{1p,1h}\rangle. \tag{5}$$

At small excitation energies these particle-hole states have long lifetimes, and following Landau they are called states with quasiparticles and holes.

In Landau theory the correlated $|\tilde{\Psi}_0\rangle$ is assumed to be the exact ground state, and the low-energy $|\tilde{\Psi}_{np,nh}\rangle$ states with n quasi-particle-hole pairs are semistationary states. The CB states are generally not eigenstates of H since they include only the dominant correlations in an approximate form. Feenberg [13] argued that the Hamiltonian matrix will have smaller nondiagonal elements in the CB since $|\Psi_X\rangle$ are much closer to the exact $|\tilde{\Psi}_X\rangle$ than the $|\Phi_X\rangle$. Therefore many-body perturbation theory could have better convergence in the CB. The CBT has been used to study various properties including optical potentials of nucleons in SNM [14] and responses of SNM [15].

A. Effective interaction

The energy of the correlated state $|\Psi_X\rangle$ is

$$\langle\Psi_X|H|\Psi_X\rangle = \frac{\langle\Phi_X|[\mathcal{S}\Pi F_{ij}](H - T_{FG}(X))[\mathcal{S}\Pi F_{ij}]|\Phi_X\rangle}{\langle\Phi_X|[\mathcal{S}\Pi F_{ij}]^2|\Phi_X\rangle} + T_{FG}(X), \tag{6}$$

$$T_{FG}(X) = \sum_{\text{all } i \text{ occupied in } \Phi_X} \frac{k_i^2}{2m}. \tag{7}$$

Including only two-body clusters:

$$\langle\Psi_X|H|\Psi_X\rangle = T_{FG}(X) + \sum_{i<j} \langle ij - ji|F_{ij}\left[v_{ij}F_{ij} - \frac{1}{m}(\nabla^2 F_{ij}) - \frac{2}{m}(\boldsymbol{\nabla} F_{ij}) \cdot \boldsymbol{\nabla}\right]|ij\rangle, \tag{8}$$

where $|ij\rangle = e^{i(\mathbf{k}_i \cdot \mathbf{r}_i + \mathbf{k}_j \cdot \mathbf{r}_j)}\chi_{\sigma\tau}(i)\chi_{\sigma\tau}(j)$, $\chi_{\sigma\tau}$ denote spin-isospin states, and v_{ij} is taken to be the static part of the Argonne $v8'$ potential. The gradient operates on the relative coordinate, and the sum $i<j$ is over states occupied in $|\Phi_X\rangle$. The effective correlated basis two-nucleon interaction is given by

$$v_{ij}^{CB} = F_{ij}\left[v_{ij}F_{ij} - \frac{1}{m}(\nabla^2 F_{ij}) - \frac{2}{m}(\boldsymbol{\nabla} F_{ij}) \cdot \boldsymbol{\nabla}\right]. \tag{9}$$

The v_{ij}^{CB} has momentum dependence via the $(\boldsymbol{\nabla} F_{ij}) \cdot \boldsymbol{\nabla}$ term, which gives contributions to the matter energy via exchange terms in Eq. (8). This contribution is much smaller than that of the momentum independent, static terms in v_{ij}^{CB} defined as

$$v_{ij}^{CBS} = F_{ij}\left(v_{ij} - \frac{1}{m}\nabla^2\right)F_{ij}. \tag{10}$$

We consider only v_{ij}^{CBS} in this work.

The energy expectation value [Eq. (6)] has contributions from clusters with $\geqslant 3$ nucleons [16]. They contribute to the two-body v_{ij}^{eff} as well as $\geqslant 3$-body effective interactions such as V_{ijk}^{eff}. Their contribution to v_{ij}^{eff} has been studied in the past [14]. These many-body cluster contributions are mostly neglected or approximated in the present work for the following reasons.

The low-energy responses to weak currents are expected to be sensitive to the spin, isospin, and Gamow-Teller susceptibilities of matter. The isospin susceptibility of nuclear matter and the spin susceptibility of pure neutron matter, calculated using the present two-body v_{ij}^{CBS} agree well with results of recent many-body calculations [9]. In addition, the calculated spin and Gamow-Teller susceptibilities of nuclear matter are similar to those obtained with some recent Skyrme-like and Michigan three-range Yukawa interactions [17]. Thus it appears that the spin-isospin dependent parts of the present v_{ij}^{CBS} provide a good approximation.

However, the matter energy calculated using v^{CBS} has a minimum at $\rho \gg \rho_0$ and matter is unstable at $\rho = \rho_0$. In fact,

we believe that SNM is stable to density fluctuations down to densities ~ 0.1 fm^{-3} [18]. We must ultimately include the three-body bare and effective forces and many-body cluster terms in the effective forces to obtain this stability. In the total energy, $E(\rho)$, of SNM there is a large cancellation between the contributions of the one-body T_{FG} and two-body v_{ij}^{eff}. Therefore the contributions of many-body clusters to the $E(\rho)$ are important. In the absence of these, the response of density fluctuations to the spin and isospin independent part of O_{NV} cannot be calculated. For calculating neutrino scattering processes via the density term of O_{NV}, we add a correction to v^{CBS} that stabilizes matter at $\rho \gtrsim 0.1$ fm^{-3} and reproduces the empirical $E(\rho)$ of Ref. [18]. This correction to v^{CBS} is discussed in more detail in Sec. V. It does not contribute to the dominant charge current and the spin and/or isospin dependent parts of neutral current response of matter.

B. Effective weak operators

The effective weak operators, O_W^{eff}, are defined as

$$\langle \Psi_F|O_W|\Psi_I\rangle = \frac{\langle \Phi_F|[\mathcal{S}\Pi F_{ij}]O_W[\mathcal{S}\Pi F_{ij}]|\Phi_I\rangle}{\sqrt{\langle \Phi_F|[\mathcal{S}\Pi F_{ij}]^2|\Phi_F\rangle\langle \Phi_I|[\mathcal{S}\Pi F_{ij}]^2|\Phi_I\rangle}} \equiv \langle \Phi_F|O_W^{eff}|\Phi_I\rangle. \quad (11)$$

Here subscripts I and F label the initial and final states of nuclear matter and O_W are the bare low energy one-body weak operators given by

$$O_F = \sum_i O_F(i) = \sum_i \tau_i^{\pm} e^{i\mathbf{q}\cdot\mathbf{r}_i}, \quad (12)$$

$$\mathbf{O}_{GT} = g_A \sum_i \mathbf{O}_{GT}(i) = g_A \sum_i \tau_i^{\pm}\sigma_i e^{i\mathbf{q}\cdot\mathbf{r}_i}, \quad (13)$$

$$O_{NV} = \sum_i O_{NV}(i) = \sum_i \left(-\sin^2\theta_W + \frac{1}{2}(1-2\sin^2\theta_W)\tau_i^z\right)e^{i\mathbf{q}\cdot\mathbf{r}_i}, \quad (14)$$

$$\mathbf{O}_{NA} = g_A \sum_i \mathbf{O}_{NA}(i) = g_A \sum_i \frac{1}{2}\tau_i^z\sigma_i e^{i\mathbf{q}\cdot\mathbf{r}_i}, \quad (15)$$

i is the nucleon number label and $\mathbf{q}$ is the momentum given by the weak boson to the nucleon. The electroweak mixing angle is θ_W with $\sin^2\theta_W = 0.2314$, and $g_A = 1.26$ is the ratio of the weak axial vector and Fermi coupling constants of the nucleon. The four operators are called Fermi (F), Gamow-Teller (GT), neutral-vector (NV) and neutral-axial-vector (NA).

Note that O_W^{eff} is a many-body operator: $O_W^{eff} = O_W^{eff(1b)} + O_W^{eff(2b)} + \cdots$. We define the $O_W^{eff(nb)}$ operator such that it contributes to the matrix element of O_W [Eq. (11)] only when $|\Phi_F\rangle$ is an n-particle-hole excitation of $|\Phi_I\rangle$:

$$|\Phi_F\rangle = a_{p_1}^\dagger a_{p_2}^\dagger \cdots a_{p_n}^\dagger a_{h_n}\cdots a_{h_2}a_{h_1}|\Phi_I\rangle. \quad (16)$$

The $O_W^{eff(nb)}$ is then an n-quasiparticle operator. The dominant part of the weak response of SNM comes from the $1p$-$1h$ excitations:

$$|\Phi_F\rangle = a_{\mathbf{p},\sigma_p,\tau_p}^\dagger a_{\mathbf{h},\sigma_h,\tau_h}|\Phi_I\rangle, \quad (17)$$

to which only the $O_W^{eff(1b)}$ contributes. The total response has smaller contributions from $n \geqslant 2$ quasi-particle-hole excitations via $O_W^{eff(n\geq 2b)}$. In Sec. IX A we study sums and energy weighted sums of the weak response. They suggest that the $n \geqslant 2$ quasi-particle-hole excitations contribute mostly to response at large excitation energy, and their effect on the NMFP in SNM should be small. From now on we consider only the $O_W^{eff(1b)}$ and drop the $(1b)$ superscript for brevity.

The cluster expansion [9,16] is used to calculate the O_W^{eff} from Eq. (11). The one-body cluster contributions give $O_W^{eff} = O_W$; however, $\geqslant$2-body clusters make $O_W^{eff} \neq O_W$. In I, the effective one-body operators were calculated in a two-body cluster approximation at a variety of proton fractions and matter densities $\left(\rho = \frac{1}{2}, 1, \frac{3}{2}\rho_0\right)$. It is convenient to define a quenching factor, $\eta = |\langle \Phi_F|O^{eff}|\Phi_I\rangle|^2 / |\langle \Phi_F|O^{bare}|\Phi_I\rangle|^2$ to characterize the difference between the bare and effective operators. For isospin and spin dependent operators, O^{eff} is quenched relative to O^{bare} and $\eta \sim 0.75-0.80$. For these operators, η is relatively insensitive to the system density. However, for the isospin and spin independent term of O_{NV}, $e^{i\mathbf{q}\cdot\mathbf{r_i}}\sin^2\theta_W$, η is very sensitive to the density of the system; at $\rho = (1/2)\rho_0$, the effective operator is enhanced and $\eta \sim 1.2$ while at $\rho = (3/2)\rho_0$ it is suppressed with $\eta \sim 0.75$. For all of the effective weak operators η is essentially independent of q at low momentum transfers but depends slightly ($<3\%$) on the initial and final momenta, $\mathbf{h}$ and $\mathbf{p}$, via the exchange terms of the cluster expansion of O_W^{eff} obtained from Eq. (11).

III. RESPONSE FUNCTIONS IN THE TAMM-DANCOFF APPROXIMATION

We begin by calculating the response to weak probes of cold SNM defined for vector currents as

$$R_V(\omega,q) = \frac{1}{A}\sum_F |\langle \Psi_F|O_V|\Psi_I\rangle|^2 \delta(\omega + E_I - E_F) \quad (18)$$

$$= \frac{1}{A}\sum_F |\langle \Phi_F|O_V^{eff}|\Phi_I\rangle|^2 \delta(\omega + E_I - E_F). \quad (19)$$

Here ω is the energy transfer and A the total number of nucleons. For axial-vector currents it is

$$R_{AV}(\omega,q) = \frac{1}{A}\sum_{\alpha=x,y,z}\sum_F |\langle \Phi_F|O_{AV,\alpha}^{eff}|\Phi_I\rangle|^2 \delta(\omega + E_I - E_F), \quad (20)$$

where α denotes the components of the axial vector.

The ground state is approximated as $|\Psi_I\rangle = (\mathcal{S}\Pi F)|\Phi_0\rangle$. In the zeroth order of CBT, $v^{eff} = 0$, the states $|\Psi_F\rangle$ are single quasi-particle-hole excitations:

$$|\Psi_F\rangle = |\Psi_{mi}\rangle = (\mathcal{S}\Pi F)|\Phi_{mi}\rangle = (\mathcal{S}\Pi F)a_m^\dagger a_i|\Phi_0\rangle. \quad (21)$$

We use subscripts $m,n,\ldots$ to denote the particle and $i,j,\ldots$ to denote hole states. The zeroth-order CBT response is given by

$$R_V^{(0)}(\omega,\mathbf{q}) = \frac{1}{A}\sum_{k_i\leq k_F} |\langle\Phi_{mi}|O_V^{eff}(\mathbf{k}_m,\mathbf{k}_i,\rho)|\Phi_0\rangle|^2 \delta(\epsilon_m^{(0)} - \epsilon_i^{(0)} - \omega) \times \delta^3(\mathbf{k}_m - \mathbf{k}_i - \mathbf{q}), \quad (22)$$

for example. The single-particle energies

$$\epsilon_a^{(0)} = \frac{k_a^2}{2m} \quad (23)$$

for $a=m$ or i, since $v^{eff}=0$. The $R_V^{(0)}(\omega,\mathbf{q})$ differs from the FG response only via O_V^{eff}. In Eq. (22) we have clearly indicated the dependence of O^{eff} on $\mathbf{k}_m,\mathbf{k}_i$ and the matter density ρ. It is omitted from the following equations just for brevity.

In the first order of CBT the states $|\Psi_I\rangle$ and $|\Psi_F\rangle$ retain their simple form as in the mean-field or Hartree-Fock (HF) approximations of the many-body theory. The correlated HF (CHF) response is obtained by using the CHF quasiparticle energies in Eq. (22). Within the present approximations they are given by

$$\epsilon_a = \epsilon_a^{(0)} + \sum_{k_i\leq k_F} \langle ai - ia|v^{CBS}|ai\rangle. \quad (24)$$

The Tamm-Dancoff approximation provides the next step in the calculation of response functions. The ground state retains it's simple form; however, the excited states, $|\Psi_F\rangle$, are expanded in a basis of correlated $1p$-$1h$ excitations with total momentum $\mathbf{q}$, isospin $T=0,1$, and spin $S=0,1$:

$$|\Psi_F\rangle = (\mathcal{S}\Pi F)\sum_{mi} c_{mi}^F a_m^\dagger a_i|\Phi_0\rangle = (\mathcal{S}\Pi F)\sum_{mi} c_{mi}^F|mi\rangle. \quad (25)$$

The coefficients, c_{mi}^F, are obtained by diagonalizing the Hamiltonian in the correlated $1p$-$1h$ basis. We refer to this method as CTDA.

The matrix elements of the Hamiltonian between $1p$-$1h$ states mi and nj are given by

$$H_{mi,nj} = (\epsilon_m - \epsilon_i)\delta_{ij}\delta_{mn} + \langle mj|v^{CBS}|in\rangle - \langle jm|v^{CBS}|in\rangle. \quad (26)$$

In the CTDA the effective interaction between quasi-particle-hole pairs is treated to all orders. This is necessary because this interaction can produce collective coherent states.

We model the infinite system in a box with sides L using periodic boundary conditions. The single particle states are

$$\phi_i = \frac{1}{\sqrt{V}} e^{i\,\mathbf{k}_i\cdot\mathbf{r}_i}\chi_{\sigma\tau}(i), \quad (27)$$

where $\mathbf{k}_n=(2\pi/L)\mathbf{n}$ and $n_{x,y,z}=(0,\pm1,\pm2\ldots)$. At zero temperature, all single-particle states with $|\mathbf{k}_i|\leq k_F$ are occupied in the ground state. The $1p$-$1h$ excitations consist of all states $|mi\rangle$ where $|\mathbf{k}_m|=|\mathbf{k}_i+\mathbf{q}|>k_F$. For the states $\mathbf{k}_m$ to be on the lattice of momentum states in the box, given that $\mathbf{k}_i$ are on the lattice, we must have

$$\mathbf{q} = \frac{2\pi}{L}(n_{q,x}\hat{\mathbf{x}} + n_{q,y}\hat{\mathbf{y}} + n_{q,z}\hat{\mathbf{z}}), \quad (28)$$

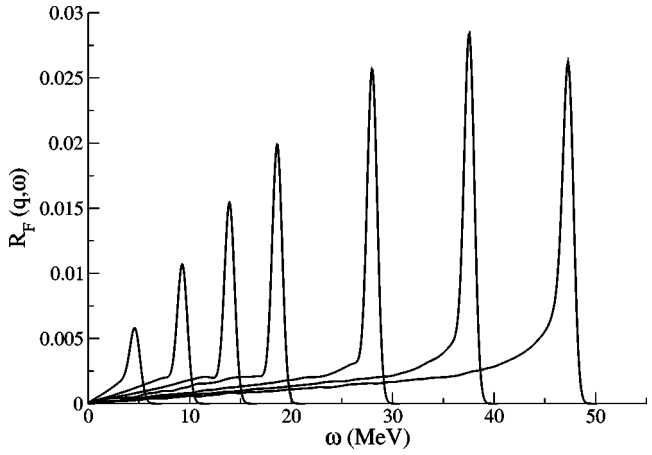

FIG. 1. Fermi response functions calculated for cold SNM at $\rho=\rho_0$ using CTDA, v^{CBS}, and O^{eff} at $q=0.05$, 0.10, 0.15, 0.20, 0.30, 0.40, and 0.50 fm^{-1}. The width of the Gaussian folding function is 0.7 MeV.

$$L = \frac{2\pi}{|q|}\sqrt{n_q^2}. \quad (29)$$

This gives a minimum box length $L_{min}=2\pi/|q|$. The size of the basis is increased by increasing n_q^2. By adopting the box method, the exchange terms of Eq. (26) are trivially and explicitly included and we hope that calculations at finite temperature will be simpler.

The response functions, Eqs. (19) and (20), obtained by diagonalizing the Hamiltonian matrix [Eq. (26)] between all the p-h states in the periodic box are a series of delta functions with various strengths. For graphing and fitting purposes, these delta functions have been folded with a Gaussian function. The width of the folding function was chosen to best reproduce the analytic noninteracting FG calculations. However, the width is not a physical parameter and observables such as the NMFP must not be sensitive to it. In practice, this is true if one uses small enough widths such as those chosen here.

IV. CHARGE CURRENT RESPONSE FUNCTIONS

The absorption of neutrinos via the charged current process $n+\nu_e\rightarrow p+e^-$ is determined by the Fermi and Gamow-Teller (GT) responses of nuclear matter. The results obtained in the CTDA for $\rho=\rho_0$ are shown in Figs. 1 and 2 for various values of $\mathbf{q}$. In Figs. 3 and 4 we give more details of the responses at $q=0.3$ fm^{-1}. The top graphs of Figs. 3 and 4 show the response functions across all energy transfers ω; the lower, a magnification of the small ω region. In both figures, $\mathbf{q}=|q|(1/\sqrt{14})(\hat{\boldsymbol{x}}+2\hat{\boldsymbol{y}}+3\hat{\boldsymbol{z}})$ with L chosen such that the number of $1p$-$1h$ basis states is $\sim$3200 and the box contains $\sim$77 000 nucleons.

The response functions indicated by cross marks in Figs. 3 and 4 are for noninteracting nucleons in the periodic box. It is clear that the box is large enough to well reproduce the analytic result [19] indicated by a thick solid line. The zeroth-order response (plus marks) is included to illustrate

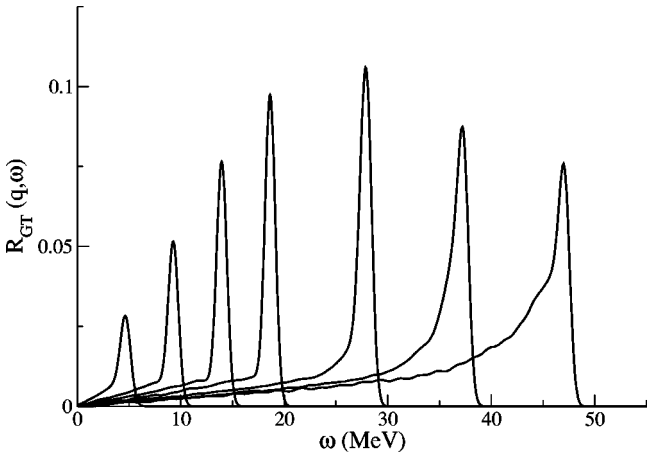

FIG. 2. Gamow-Teller response functions calculated for cold SNM at $\rho=\rho_0$ using CTDA, v^{CBS} and O^{eff} at $q=0.05$, 0.10, 0.15, 0.20, 0.30, 0.40, and 0.50 fm^{-1}. The width of the Gaussian folding function is 0.7 MeV.

that the use of the effective operator suppresses the response by $\sim 20-25$ %.

Also shown in Figs. 3 and 4 are the response functions calculated using O^{eff} with various common assumptions made regarding v^{eff}. The CHF approximation, which is equivalent to including only the diagonal matrix elements of v^{CBS}, is indicated by the dashed line. Results including only direct terms of v^{CBS} in the off-diagonal matrix elements of the CTDA are shown by the dotted line. The thin solid line shows the response using v^{CBS} and the full CTDA equation. All three calculations indicate that interactions shift the strength to higher ω when compared to the noninteracting FG. However, the CHF response is almost twice as strong at low ω. In addition, for R_F, only the full CTDA calculation using v^{CBS} gives a coherent state outside of the *p-h* continuum, indicating that the exchange terms are not negligible. This is not the case for R_{GT}, where the exchange terms have little effect. The width of the coherent state in Figs. 3 and 4 indicates the width of the folding function used in these figures.

The three GT responses corresponding to $\alpha=x,y,z$ [Eq. (20)] are classified as spin longitudinal ($\alpha=z$) and two spin transverse ($\alpha=x,y$), where the direction of **q** defines the z axis [10,20,21]. The peak of R_{GT} in Fig. 4 has contributions from three states that lie just beyond the *p-h* continuum. The one at relatively lower energy is from the longitudinal response while the other two are from the transverse and are degenerate. The ground state of uniform FG has $J_z=0$, and conservation of J_z implies that only states with $J_z=0$ contribute to the longitudinal response. However, resonant states obtained using a finite box are not eigenstates of J_z. For the box lengths used in the present calculation at least 99% of the strength of each resonance can be attributed to either the spin longitudinal or spin transverse directions. As q is increased, the peaks are shifted into the *p-h* continuum and distinguishable resonances disappear.

Calculations that assume a bare weak operator and Skyrme-like effective interactions without tensor forces use a slightly different definition of R_{AV}. The three directions, α

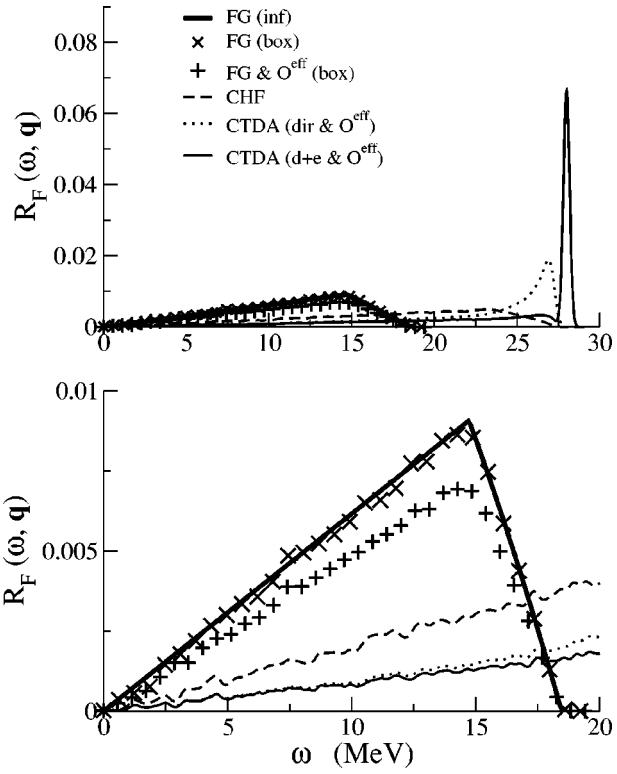

FIG. 3. Fermi response functions calculated at $q=0.3$ fm^{-1} for cold SNM at $\rho=\rho_0$. The upper graph shows the full response across all values of ω, the lower is a magnification of the small ω region. The thick solid line is the analytic result for an infinite noninteracting FG [19] while the cross marks show the response obtained using the finite periodic box. The zeroth-order response obtained by replacing O^{bare} by O^{eff} in the noninteracting FG is indicated by the plus marks. The remaining lines are calculations using O^{eff} and various approximations: dashed, CHF; dotted, includes only direct v^{CBS} off-diagonal matrix elements, and solid, full CTDA using v^{CBS}. The curves show responses folded with a Gaussian of width 0.28 MeV.

$=x,y,z$ in Eq. (20) are equivalent in the absence of tensor forces. In this case it is most convenient to calculate the response in one direction, $\alpha=z$ for example. However, experimental and theoretical investigations of the isovector $(\vec{p},\vec{n})$ reactions indicate an enhancement in the longitudinal response [10,20,21] due to the one-pion exchange, tensor interaction. The spin longitudinal and spin transverse components of the axial-vector response functions can differ significantly at larger values of q and must be calculated separately. We have chosen here to sum the components of the axial vectors and discuss the *total* response. The differences in the sums of spin longitudinal and transverse responses will be discussed in Sec. IX. A third of the present R_{AV} should be used to compare results with those of simpler models that ignore tensor forces.

V. NEUTRAL CURRENT RESPONSE FUNCTIONS

For the neutrino scattering processes, $N+\nu_e \rightarrow N'+\nu_e'$ ($N=n$ or p), two transitions are possible: isospin change ΔT

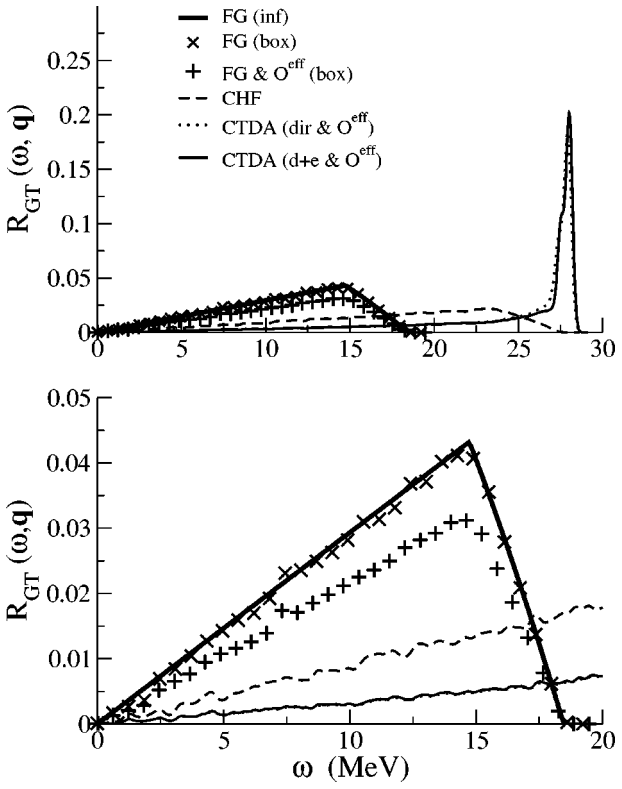

FIG. 4. Gamow-Teller response functions calculated at $q=0.3$ fm^{-1} for cold SNM at $\rho=\rho_0$. See caption of Fig. 3 for notation.

$=0$ and 1. For $\Delta T=1$, only the τ_z terms of the neutral current operators can contribute. For SNM, these can be trivially related to the charge current operators discussed in Sec. IV: the $\Delta T=1$ contribution to $R_{NV}=1/2(1-2\sin^2\theta_W)^2R_F$ and all of $R_{NA}=1/2R_{GT}$. We do not include separate results for these response functions.

For $\Delta T=0$ transitions, the neutral current response function is given by the isospin and spin independent operator of O_{NV}, $\Sigma_i \sin^2\theta_W e^{i\mathbf{q}\cdot\mathbf{r}_i}$ where $\Sigma_i e^{i\mathbf{q}\cdot\mathbf{r}_i}$ is the density operator. The total energy, $E(\rho)$, calculated in I using v^{CBS}, minimizes at $\rho \gg \rho_0$ and matter is unstable to density fluctuations at the densities considered in this work. However, it is believed that matter is stable down to densities ~ 0.1 fm^{-3} [18]. We therefore add a correction to v^{CBS} meant to take into account the neglected three-body forces and many-body cluster contributions. This correction is chosen to reproduce the semiempirical $E(\rho)$ in Ref. [18].

We use a density dependent zero-range central interaction, which is to be used only for direct matrix elements,

$$v_{ij}^{\delta}(\rho)=\left[C_1\left(\frac{\rho}{\rho_0}\right)^{\alpha}+C_2\right]\delta(\mathbf{r}_i-\mathbf{r}_j), \tag{30}$$

to represent this correction. For finite range effective interactions such as v^{CBS}, the exchange contribution to the matrix element of the Hamiltonian depends on the momentum difference between the hole states, $\mathbf{k}_{ij}=\mathbf{k}_i-\mathbf{k}_j$. When $|\mathbf{k}_{ij}|$ is large, the contribution of the exchange term to the effective interaction is negligible. However, for δ-function interactions the exchange contribution is a constant, independent of the relative momenta. Including exchange contributions from $v^{\delta}(\rho)$ causes unphysically large corrections in the exchange channel and we therefore assume that $v^{\delta}(\rho)$ contributes only to the direct matrix elements.

TABLE I. Parameters of v_{ij}^{δ} at $\rho=0.16$ and 0.24 fm^{-3}.

ρ	C_1	C_2	α
0.16	310.3	−302.4	0.54
0.24	342.7	−356.0	0.50

The contribution of $v^{\delta}(\rho)$ to the energy of matter per nucleon is

$$\frac{E^{\delta}(\rho)}{A}=\frac{1}{2}\sum_{i,j}\langle ij|v_{ij}^{\delta}(\rho)|ij\rangle \tag{31}$$

$$=\frac{1}{2}\left[C_1\left(\frac{\rho}{\rho_0}\right)^{\alpha}+C_2\right]\rho. \tag{32}$$

The parameters C_1, C_2, and α are chosen so that $v^{CBS}+v^{\delta}(\rho)$ reproduces the semiempirical $E(\rho)$ of Ref. [18] in the $(1/2-3/2)\rho_0$ range. The fitted parameters are given in Table I at the two densities considered. Recall that v^{CBS} is density dependent because the correlation functions that define v^{CBS} are density dependent. The parameters of $v_{ij}^{\delta}(\rho)$ therefore depend on the density at which v^{CBS} is determined. However, both sets fit the same $E(\rho)$, and predict similar responses.

The contribution of $v^{\delta}(\rho)$ to the energy of single-particle states, ϵ^{δ}, is obtained by differentiating $E^{\delta}(\rho)/V$ with respect to ρ, and the second derivative with respect to ρ is the effective interaction:

$$\epsilon^{\delta}=\frac{1}{2}\left[C_1(\alpha+2)\rho_0\left(\frac{\rho}{\rho_0}\right)^{\alpha+1}+2C_2\rho\right] \tag{33}$$

$$\langle mj|v_{eff}^{\delta}|in\rangle=\frac{1}{V}\frac{1}{2}\left[C_1(\alpha+2)(\alpha+1)\left(\frac{\rho}{\rho_0}\right)^{\alpha}+2C_2\right]. \tag{34}$$

The $\langle mj|v_{eff}^{\delta}|in\rangle$ is of the same order as $\langle mj|v_c^{CBS}|in\rangle$ in $\Delta T=0$, NV transitions.

The neutral current $\Delta T=0$ response functions at $q=0.30$ fm^{-1} for $\rho=\rho_0$ and $(3/2)\rho_0$ are given in Fig. 5. The calculations have been scaled by 1,000 for convenience. The matter is unstable at $\rho=(1/2)\rho_0$ and we have not included response functions for this density. The dotted lines show $\Delta T=0$ R_{NV} for a non-interacting FG, the CTDA response functions obtained using $v^{CBS}+v^{\delta}(\rho)$ are shown as the dashed line when O^{bare} is used and solid when O^{eff} is used. The density response is pushed to larger ω though not as much as the R_F and R_{GT}. And the suppression due to O^{eff} depends sensitively on the system density. At $\rho=\rho_0$, there is little suppression while at $\rho=(3/2)\rho_0$, the response is quenched by $\sim 25\%$.

The present treatment of the density response is less satisfactory than that of the other responses. However, the ΔT

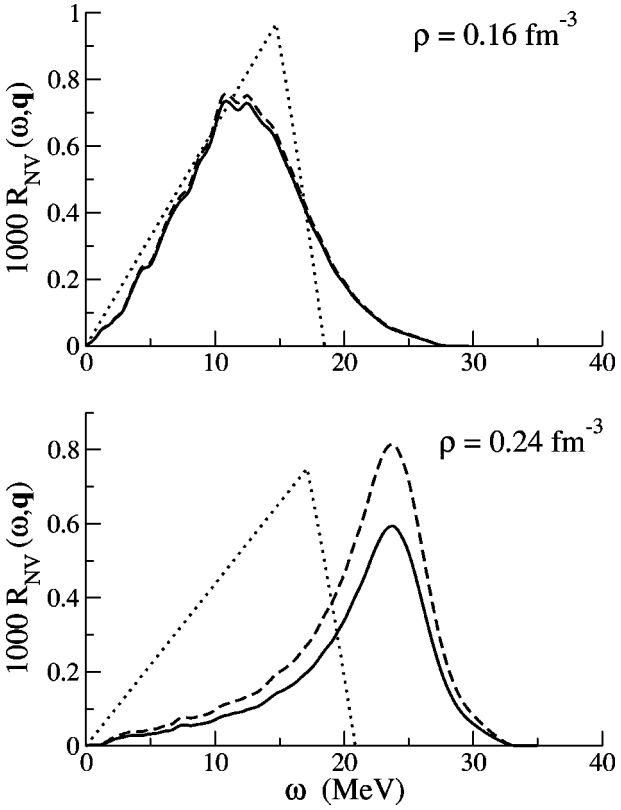

FIG. 5. Neutral current response functions for $\Delta T=0$ transitions calculated at $q=0.3$ fm^{-1} for cold SNM at $\rho=\rho_0$ (upper) and $(3/2)\rho_0$ (lower). Dotted lines show the response for a noninteracting FG. Response functions calculated in TDA using v^{CBS} and O^{bare} are shown as dashed lines and the CTDA results with O^{eff} by solid lines. The curves show responses folded with a Gaussian of width 0.96 MeV for $\rho=\rho_0$ and 1.2 MeV for $\rho=(3/2)\rho_0$.

$=0$ neutral current response gives a contribution only of order 10% to the total neutrino scattering cross section. The overall accuracy of the present calculation is also of order 10%.

VI. NEUTRINO MEAN FREE PATHS

To evaluate the significance of these changes to the response functions, we calculate the NMFP for low energy neutrino scattering and neutrino absorption processes in cold SNM. For the low energy neutrino reactions considered, the Hamiltonian density is given by the Weinberg-Salam model:

$$H_W=\frac{G_F}{\sqrt{2}}\int d^3x e^{i\mathbf{q}\cdot\mathbf{x}}\ell_\mu\, j^\mu(x), \tag{35}$$

where $\ell_\mu=\overline{\psi_2}\gamma_\mu(1-\gamma_5)\psi_1$ is the lepton current, the subscripts 1,2 denote the incident and outgoing leptons, respectively, and $\mathbf{q}=\mathbf{p}_1-\mathbf{p}_2$. The nonrelativistic nuclear current, $j^\mu_{fi}=(j^0,\mathbf{j})$, is defined as

$$j^0=\langle\Psi_F|O_V|\Psi_I\rangle, \tag{36}$$

$$\mathbf{j}=\langle\Psi_F|O_{AV}|\Psi_I\rangle. \tag{37}$$

$G_F=1.166\ x\ 10^{-5}$ GeV^{-2}. The cross section is obtained using Fermi's golden rule and averaging over initial and summing over final spin states:

$$\frac{d\sigma}{d^3p_2}=\frac{G_F^2}{(2\pi)^2}\sum_F\delta(\omega+E_I-E_F)\frac{1}{E_1E_2}[p_1^\mu p_2^\nu+p_1^\nu p_2^\mu - p_1\cdot p_2 g^{\mu\nu}+i\epsilon^{\mu\alpha\nu\beta}p_1^\alpha p_2^\beta]j^\mu_{fi}j^{\nu*}_{fi}, \tag{38}$$

where $\epsilon^{\sigma\alpha\tau\beta}$ is the antisymmetric tensor with $\epsilon^{0123}=1$.

We choose the z axis in the direction of $\mathbf{q}$, $q^\mu=(p_1-p_2)^\mu=(\omega,0,0,q)$ and define $Q^\mu=(p_1+p_2)^\mu=(\Omega,Q_x,0,Q_z)$. Equation (38) then simplifies to

$$\frac{d\sigma}{d^3p_2}=\frac{G_F^2}{(2\pi)^2}\sum_F\delta(\omega+E_I-E_F)\Big[(1+\cos\theta_{12})j_0j_0^* + (1-\cos\theta_{12})\mathbf{j}\cdot\mathbf{j}^*+\frac{1}{2E_1E_2}[Q_x^2j_xj_x^*+(Q_z^2-q^2)j_zj_z^* + Q_xQ_z(j_xj_z^*+j_zj_x^*)]\Big], \tag{39}$$

where, in the $m_e=0$ limit, the lepton scattering angle is given by $\cos\theta_{12}=(E_1^2+E_2^2-q^2)/(2E_1E_2)$.

Using the previous definitions of the response functions, Eqs. (19) and (20), and further defining a mixed component response,

$$R_{AV,ij}(\omega,\mathbf{q})=\frac{1}{A}\sum_F\langle\Phi_I|O^{eff\dagger}_{AV,i}|\Phi_F\rangle\langle\Phi_F|O^{eff}_{AV,j}|\Phi_I\rangle \times\delta(\omega+E_I-E_F), \tag{40}$$

where i and j are components of the axial-vector operator, the cross section can be expressed in terms of the ω-q space

$$\frac{d\sigma}{dqd\omega}=\frac{G_F^2}{2\pi}\frac{E_2}{E_1}q\Big\{(1+\cos\theta_{12})R_V+(1-\cos\theta_{12})R_{AV} + \frac{1}{E_1E_2}[Q_x^2R_{AV,xx}+(Q_z^2-q^2)R_{AV,zz}+2Q_xQ_zR_{AV,xz}]\Big\}. \tag{41}$$

We have made the substitution $d^3p_2=E_2^2\,dE_2\,d\Omega=[(E_1-\omega)/E_1]q\,dq\,d\omega\,d\phi$ and integrated over ϕ.

The total cross section is obtained by integrating Eq. (41) over all kinematically allowed values of ω and q. The NMFP, defined as $\lambda=(\sigma\rho)^{-1}$, is given in Figs. 6 and 7 for low energy neutrino absorption and scattering, respectively.

The top graph of Fig. 6 shows the λ_{CTDA} calculated for neutrino absorption using CTDA with v^{CBS} and O^{eff} (upper curves) as well as the λ_{FG} for a noninteracting FG (lower curves) for the densities $\rho=1/2$, 1, and $(3/2)\rho_0$ (solid, dashed, and dotted). For the absorption process, both λ_{FG} and λ_{CTDA} are dominated by R_{GT}. It accounts for $\sim$75–80 % of the total cross section of the CTDA and slightly more for the FG. The ratio $\lambda_{CTDA}/\lambda_{FG}$ is given in the bottom graph. At the densities considered, λ_{CTDA} is $\sim$2.5–3.5 times larger than λ_{FG}.

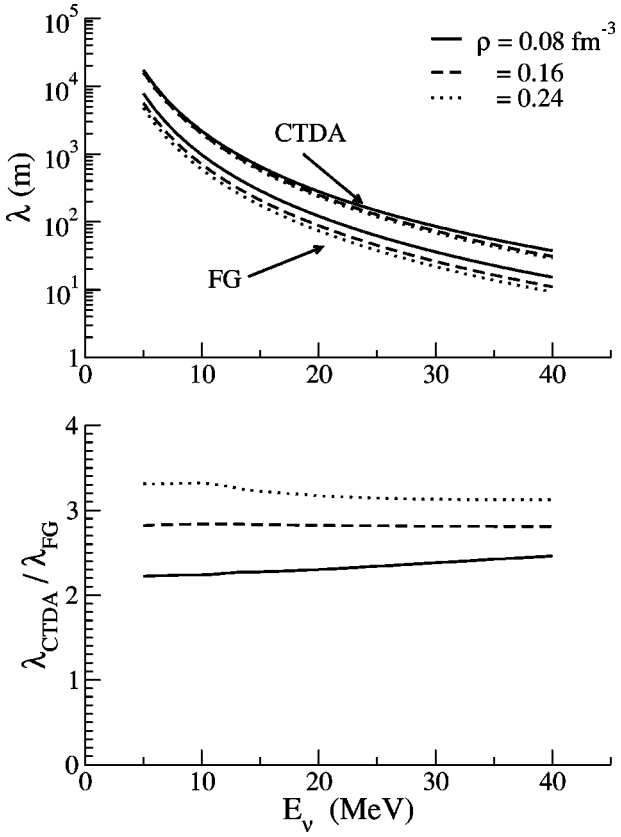

FIG. 6. NMFP for absorption, $\nu+n\rightarrow e^{-}+p$. The upper graph shows λ for a noninteracting FG (lower curves) and the CTDA (upper curves). The lower graph gives the ratio of λ_{CTDA} to λ_{FG}. The system densities are $\rho=(1/2)\rho_0$ (solid), ρ_0 (dashed), and $(3/2)\rho_0$ (dotted).

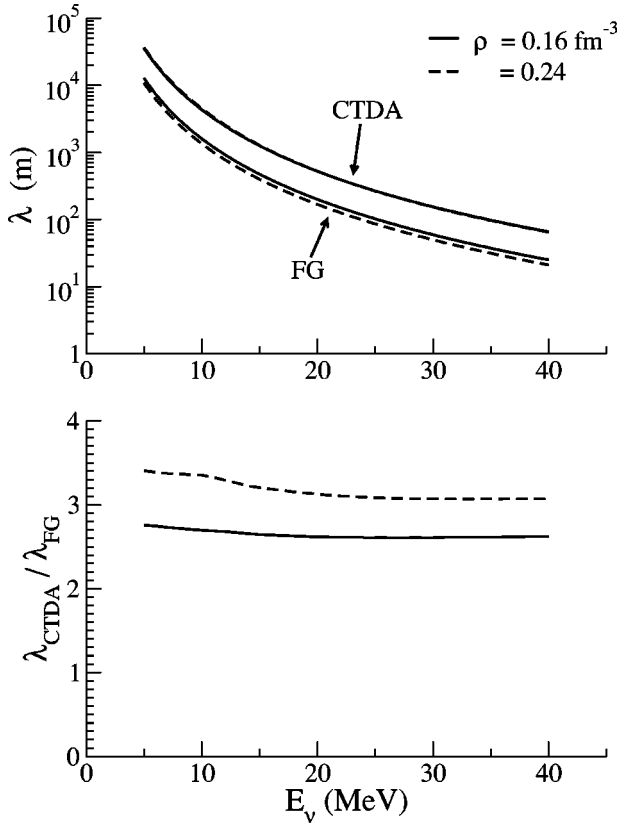

FIG. 7. NMFP for scattering, $\nu+N\rightarrow\nu'+N'$. The upper graph shows λ for a noninteracting FG (lower curves) and the CTDA (upper curves). The lower graph gives the ratio of λ_{CTDA} to λ_{FG}. The system densities are $\rho=\rho_0$ (solid) and $(3/2)\rho_0$ (dashed).

Figure 7 shows λ for neutrino scattering at $\rho=1$ and $(3/2)\rho_0$ (solid and dashed lines, respectively). As was found for the absorption process, λ_{CTDA} is $\sim 2.6-3.5$ times larger than λ_{FG}. The suppression of neutrino scattering is similar to that for absorption because the $\Delta T=1$ contribution accounts for $\sim 90\%$ of the total scattering cross section. In addition, the NMFP for scattering is ~ 2 times larger than that for absorption; the inverse of the scaling factor relating the dominant neutral and charge current axial-vector responses $[R_{NA}=(1/2)R_{GT}]$. The dominance of the $\Delta T=1$ channel ensures that errors associated with introducing the correction v^{δ} to the two-body v^{CBS} will not significantly effect the NMFP, providing that stability is ensured.

In calculating λ_{CTDA}, we have extrapolated to obtain the $q\lesssim 0.1$ fm^{-1} response functions. The side length of the box used to model the infinite system is $\propto 1/q$. For small momentum transfers, the box size becomes large and the number of basis states exceeds $\sim 10\,000$. A basis of this size is beyond the capabilities of the standard desktop computer used in this work. For this reason in Figs. 6 and 7 we have not included λ for $E_\nu<5$ MeV, which is completely determined by the extrapolated response functions. The contribution of these low q response functions becomes negligible when $E_\nu \gtrsim 20$ MeV.

In the absence of tensor forces, the low q response can be considered in two parts: a single collective state and the *p-h* continuum. In diagonalizing the Hamiltonian, all but one of the excitation energies lie within the single-particle energies of the "unperturbed" or CHF states. These states contribute to the response in the *p-h* continuum. The state with energy beyond the continuum is the collective state and its contribution to the response can be well represented by a delta function, $R_C(q)\delta(\omega-\omega_C(q))$. The energy, $\omega_C(q)$, and strength, $R_C(q)$, are linear in q when $q\lesssim 0.2$ fm^{-1}. This is illustrated in Fig. 8 where $\omega_C(q)$ (top graph) and $R_C(q)$ (middle graph) for the Fermi response R_F are plotted along with linear fits at small q. For R_{GT}, the tensor force splits the single coherent resonance into two components, spin longitudinal and spin transverse. The energies of these states remain outside of the *p-h* continuum, but have slightly different values. Each component can be fit separately using a delta function where the strength and resonant energies are linear in q at $q<0.2$ fm^{-1}.

As $q\rightarrow 0$, the response in the *p-h* continuum $[R(\omega,q)-R_C(q)\delta(\omega-\omega_C(q))]\rightarrow\alpha R^{bare}_{CHF}$. (For R_{GT} contributions of all the three resonant states are subtracted.) The coefficient α can be determined by comparing the area of $[R(\omega,q)-R_C(q)\delta(\omega-\omega_C(q))]$ to the area of R^{bare}_{CHF} calculated using O^{bare} and the CHF single-particle energies. This ratio is shown in the bottom graph of Fig. 8 for the Fermi response where

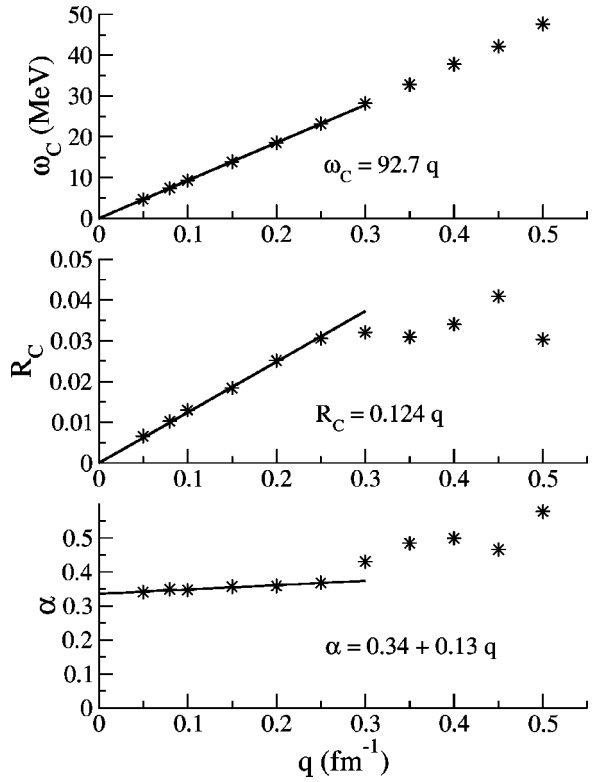

FIG. 8. Extrapolation parameters for low-q Fermi response. See text for description.

$$\alpha = \frac{\int [R(\omega,q) - R_C(q)\delta(\omega - \omega_C(q))]d\omega}{\int R^{bare}_{CHF}(\omega,q)d\omega}. \qquad (42)$$

The R^{bare}_{CHF} can be calculated analytically; at small q it depends only on the Landau effective mass. In CB theory the effective mass mostly comes from the contribution of the exchange matrix elements of v^{CBS} to the single-particle energies. It depends upon the momentum and is defined as

$$\frac{1}{m^*(k)} = \frac{1}{\hbar^2 k}\frac{d}{dk}\epsilon(k). \qquad (43)$$

The Landau effective mass, $m^*_L = m^*(k=k_F) \approx 0.64\ m_N$ at $\rho = \rho_0$ with the present v^{CBS}. This value is less than the standard value of $\sim 0.7 m_N$. However, we have not included the momentum dependence of v^{CB} nor $\geqslant$three-body contributions that are expected to increase our value of m^*_L.

Calculations that neglect tensor forces and assume O^{bare} use a simplified form of Eq. (41). In the absence of tensor forces $R_{AV,xx} = R_{AV,zz} = (1/3)R_{AV}$, and $R_{AV,xz} = 0$, and Eq. (41) can be rewritten as

$$\frac{d\sigma}{dq d\omega} = \frac{G_F^2}{2\pi}\frac{E_2}{E_1} q\left[(1 + \cos\ \theta_{12})R_V + (3 - \cos\ \theta_{12})\tfrac{1}{3}R_{AV}\right]. \qquad (44)$$

When tensor forces are included the spin longitudinal and spin transverse responses can be considerably different from $(1/3)R_{AV}$ and calculations must be carried out using Eq. (41). However, for the low energy processes ($q \lesssim 0.5$ fm^{-1}), $R_{AV,xx} \approx R_{AV,zz} \approx (1/3)R_{AV}$, and $R_{AV,xz} \approx 0$ and λ_{CTDA} calculated using Eq. (44) differs by $\lesssim 5\%$ from that calculated using the full expression for the cross section.

TABLE II. Strengths of delta function interactions for $v^{SK}(m^*)$ and $v^{SK}(m_N)$ at $\rho = \rho_0$.

	C_1	α	C_2	v^τ	v^σ	$v^{\sigma\tau}$
$v^{SK}(m^*)$	1353.07	0.25	−1982.28	183.73	60.29	257.43
$v^{SK}(m_N)$	795.55	0.36	−1271.10	269.03	145.59	342.73

VII. SKYRME-LIKE APPROXIMATIONS OF v^{eff}

Many recent calculations of NMFP have used a Skyrme-like effective interaction of the form

$$v^{SK} = (v^c + v^\tau \boldsymbol{\tau}_i \cdot \boldsymbol{\tau}_j + v^\sigma \boldsymbol{\sigma}_i \cdot \boldsymbol{\sigma}_j + v^{\sigma\tau}\boldsymbol{\sigma}_i \cdot \boldsymbol{\sigma}_j \boldsymbol{\tau}_i \cdot \boldsymbol{\tau}_j)\delta^3(\mathbf{r}_i - \mathbf{r}_j). \qquad (45)$$

Only the direct contributions of v^{SK} are used and the strengths of the delta functions can be directly related to the Landau parameters [17]. It is instructive to compare the NMFP obtained previously to that obtained by approximating v^{CBS} with this simple zero-range effective interaction. We consider two cases: the strengths of the v^{SK} interaction are fitted using an effective mass defined in the preceding section, $v^{SK}(m^*)$; and the bare nucleon mass is $v^{SK}(m_N)$.

To ensure stability, it is necessary to introduce a density dependent central interaction of the form Eq. (30) such that $v^c = v^\delta(\rho)$. Using the FG kinetic energy determined for each mass, the parameters of v^c are chosen such that the semi-empirical $E(\rho)$ in Ref. [18] is reproduced. For each mass, the strengths v^τ, v^σ and $v^{\sigma\tau}$ are fit to reproduce the susceptibilities calculated in I. The strengths of the interaction at $\rho = \rho_0$ are given in Table II.

Figure 9 compares the Fermi (upper graph) and Gamow-Teller (lower graph) TDA response functions obtained using v^{SK} and O^{eff} and v^{CBS} and O^{eff} when $q = 0.3$ fm^{-1} and $\rho = \rho_0$. For both the Fermi and GT weak operators the response obtained using $v^{SK}(m_N)$ (dashed line) is dominated by a single coherent state beyond the p-h continuum. The energy of this state is significantly less than that obtained using v^{CBS} (solid line). In contrast, R_F calculated using $v^{SK}(m^*)$ (dotted line) extends to energy transfers similar to those of the v^{CBS} calculation. However, at large q, the Landau effective mass approximation is no longer valid and differences between responses calculated with v^{CBS} and $v^{SK}(m^*)$ increase. The NMFP is most sensitive to the low ω region. In this region, $v^{SK}(m^*)$ is a good approximation to the response obtained using v^{CBS}. Similar results are obtained for R_{GT}.

In comparing v^{CBS} response functions of Fig. 9 to those of Figs. 3 and 4, the heights of the resonant peaks are significantly different. This is due to the difference in the width of the folding function used in each calculation. The Skyrme calculations contain fewer basis states requiring a larger

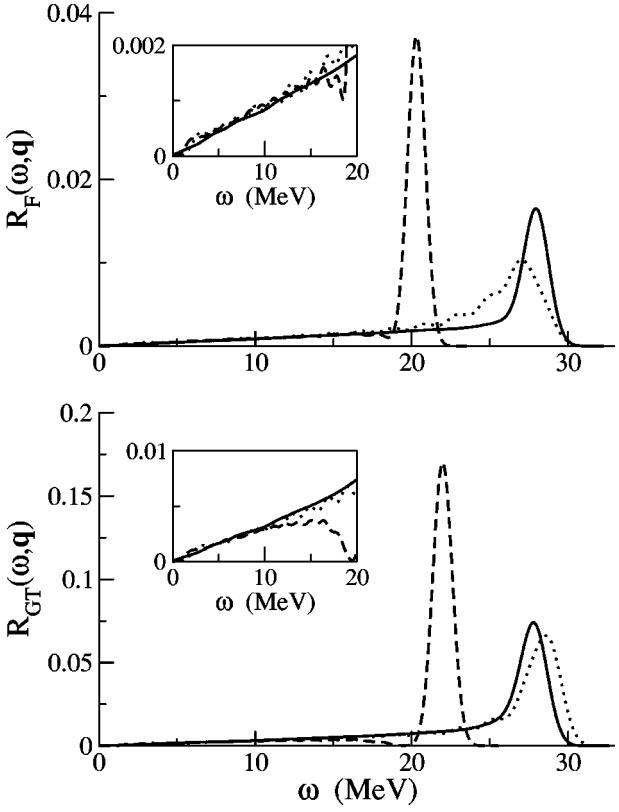

FIG. 9. Fermi (upper) and Gamow-Teller (lower) response functions calculated using $v^{SK}(m^*)$ (dotted), $v^{SK}(m_N)$ (dashed), and v^{CBS} (solid) at $q=0.3$ fm^{-1} for cold SNM at $\rho=\rho_0$. All responses have been calculated using the TDA and O^{eff}. The curves show responses folded with a Gaussian of width 1.1 MeV.

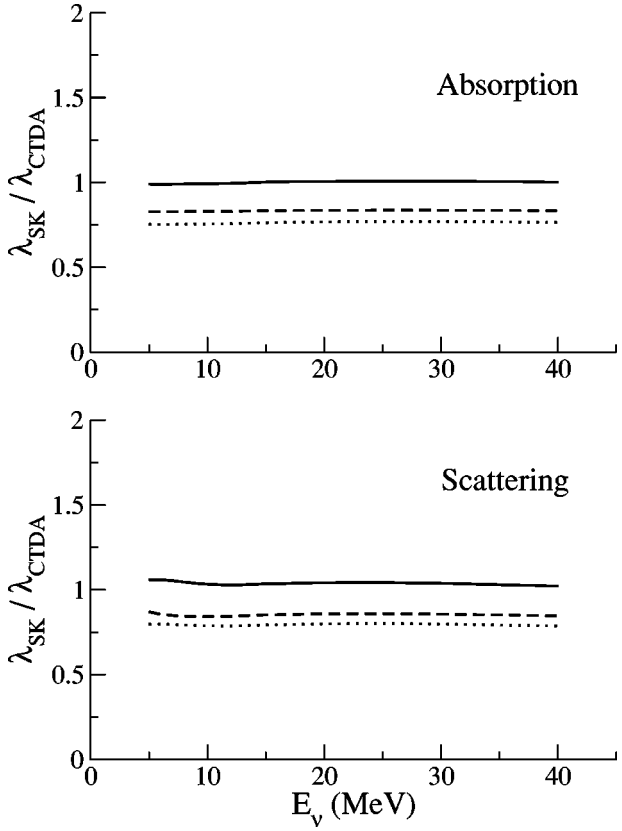

FIG. 11. NMFP for neutrino absorption (upper) and neutrino scattering (lower). Shown is the ratio of $\lambda_{SK}/\lambda_{CTDA}$ calculated in TDA using O^{eff} and $v^{SK}(m^*)$ (solid), $v^{SK}(m_N)$ (dashed). The dotted line shows the ratio calculated using $v^{SK}(m^*)$ and O^{bare}.

width to smooth the delta functions. This does not effect the calculation of physical parameters such as NMFP.

The neutral vector response for the $\Delta T=0$ transition is given in Fig. 10 for the three effective interactions. The response calculated with $v^{SK}(m_N)$ (dashed), $v^{SK}(m^*)$ (dotted), and v^{CBS} (solid) are shown for $\rho=\rho_0$ and $q=0.3$ fm^{-1}. Note

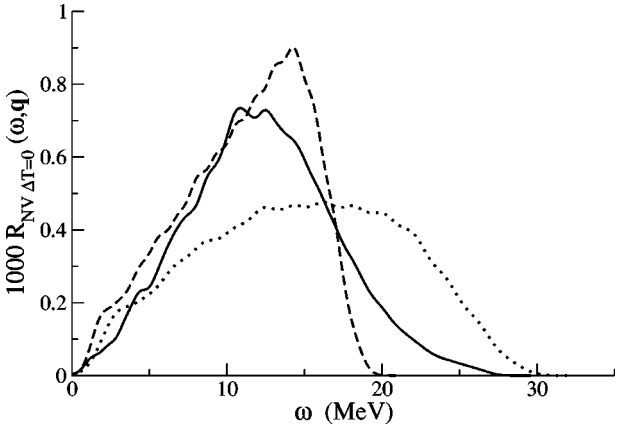

FIG. 10. $\Delta T=0$ neutral current response functions obtained using $v^{SK}(m^*)$ (dotted), $v^{SK}(m_N)$ (dashed), and v^{CBS} (solid) at $q=0.3$ fm^{-1} for cold SNM at $\rho=\rho_0$. All responses have been calculated using O^{eff} and the TDA. The curves show responses folded with a Gaussian of width 1.1 MeV.

that this response has been multiplied by 1000. The structure of the response is significantly different for each effective interaction. However, the $\Delta T=0$ contribution to the cross section is $\lesssim$10% and these differences will have little effect on the NMFP. The response functions for the $\Delta T=1$ transition are related to the charge current response functions in Fig. 9 (see Sec. V) and are not shown separately.

The ratio of the NMFP obtained using v^{SK} to those of Sec. VI at $\rho=\rho_0$ are shown in Fig. 11; $\lambda_{SK}(m^*)/\lambda_{CTDA}$ (solid line) and $\lambda_{SK}(m_N)/\lambda_{CTDA}$ (dashed line). The top graph compares results for the neutrino absorption process, the lower for neutrino scattering. For both processes, the NMFP calculated using $v^{SK}(m^*)$ is in good agreement with the results of the previous section. However, using $v^{SK}(m_N)$ underestimates the NMFP by $\sim$25%. Assuming a suitable effective mass, the zero range approximation is a fair representation of v^{CBS} for these low energy calculations.

Figure 11 also shows results obtained using $v^{SK}(m^*)$ and O^{bare}. The ratio with respect to λ_{CTDA} is shown by the dotted line. It is $\sim$25% less than the NMFP obtained when O^{eff} is used. This calculation is indicative of many current approaches and shows that calculations using an effective interaction and a bare weak operator may overestimate the neutrino cross sections.

VIII. RANDOM PHASE APPROXIMATION

The usual progression from the simple TDA calculation is to allow for $2p$-$2h$ excitations in the ground state and employ RPA. In the context of CBT, this procedure is not simple. An inherent complication of CBT is the nonorthogonality of the correlated wave functions. In the basis of uncorrelated states the ground state wave function of the RPA can be written as

$$|\Phi_{RPA}\rangle = \alpha_0|\Phi_0\rangle + \sum \alpha_{p_1p_2h_1h_2}|\Phi_{p_1p_2h_1h_2}\rangle + \cdots . \quad (46)$$

The analogous $|\Psi_{RPA}\rangle$ in correlated basis can be considered as

$$|\Psi_{RPA}\rangle = \alpha_0|\Psi_0\rangle + \sum \alpha_{p_1p_2h_1h_2}|\Psi_{p_1p_2h_1h_2}\rangle + \cdots , \quad (47)$$

where

$$|\Psi_{p_1p_2h_1h_2}\rangle = (\mathcal{S}\Pi F_{ij})a^\dagger_{p_2}a^\dagger_{p_1}a_{h_1}a_{h_2}|\Phi_0\rangle = (\mathcal{S}\Pi F_{ij})|\Phi_{p_1p_2h_1h_2}\rangle. \quad (48)$$

However, $\langle\Psi_0|\Psi_{p_1p_2h_1h_2}\rangle \neq 0$ and orthogonality corrections must be included. These corrections have been considered by Krotscheck [22] for simple Jastrow correlations using the correlated random phase approximation (CRPA).

Our objective here is to estimate the size of the RPA corrections. We therefore use $v^{SK}(m^*)$ discussed in the preceding section to calculate the response functions using RPA and determine the NMFP for neutrino absorption. The difference between TDA and RPA results with the $v^{SK}(m^*)$ should be of the order of that between CTDA and CRPA.

In RPA, the final state wave function, $|\Phi_F\rangle$, is given by

$$|\Phi_F\rangle = \left(\sum_{mi} x_{mi}\, a^\dagger_m a_i - \sum_{mi} y_{mi}\, a^\dagger_i a_m\right)|\Phi_{RPA}\rangle. \quad (49)$$

The excited states are obtained by diagonalizing the Hamiltonian in this $1p$-$1h$ basis. The resulting RPA matrix

$$\begin{pmatrix} A & B \\ -B^* & -A^* \end{pmatrix}\begin{pmatrix} X \\ Y \end{pmatrix} = \omega\begin{pmatrix} X \\ Y \end{pmatrix} \quad (50)$$

is non-Hermitian with elements defined by

$$A = (\epsilon_m - \epsilon_i)\delta_{ij}\delta_{mn} + \langle mj|v^{SK}|in\rangle, \quad (51)$$

$$B = \langle mn|v^{SK}|ij\rangle. \quad (52)$$

We again model the infinite system in a box with periodic boundary conditions containing ~40 000 nucleons.

Figures 12 and 13 compare R_F and R_{GT} at $\rho=\rho_0$ calculated using $v^{SK}(m^*)$ and O^{eff} in the RPA (solid line) and TDA (dashed line). Each figure shows the response at q values typical for the low energy processes considered. The RPA response functions are generally smaller than the TDA. The reduction of the response functions carries directly into the NMFP shown in Fig. 14. The $\lambda_{RPA}/\lambda_{FG}$ (lower graph) is ~3.6 at $\rho=\rho_0$.

In combining RPA with O^{eff} defined by CBT, we tacitly assume that effects of ground state correlations included in the RPA are not already accounted for in the O^{eff}. In the present correlated basis, the O^{eff} is dominated by tensor correlations. Recall that the quenching factor, $\eta_{GT}\approx 0.77$ for $q=0.3$ fm^{-1}. If the tensor correlations are set to zero, $\eta_{GT}\approx 1.02$, suggesting that all of the quenching is due to tensor correlations. Similar behavior is found for O^{eff}_F. The RPA using $v^{SK}(m^*)$ does not introduce tensor correlations since v^{SK} has no tensor force. However, it generates long range spin-isospin correlations in matter via the v^{SK}. Therefore it appears that the CB O^{eff} should be used in RPA calculations with Skyrme-type effective interactions, and that CRPA calculations may give ~25% longer NMFP than the present CTDA.

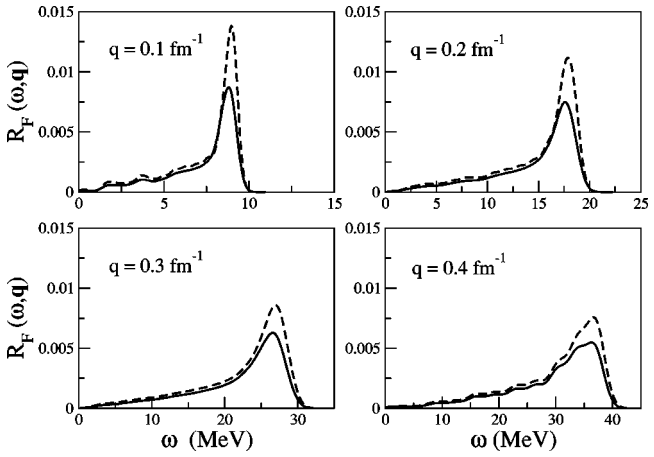

FIG. 12. Fermi response functions calculated using RPA (solid) and TDA (dashed) with O^{eff}_F and $v^{SK}(m^*)$ for $q=0.1$–0.4 fm^{-1} and $\rho=\rho_0$.

IX. SUM RULES

A. Static structure functions and energy weighted sum rules

In addition to the $1p$-h, there are multi p-h excitations that contribute to the response functions and therefore to the NMFP. So far we have neglected these contributions. We can estimate the importance of these contributions by calculating sum rules. The static structure function

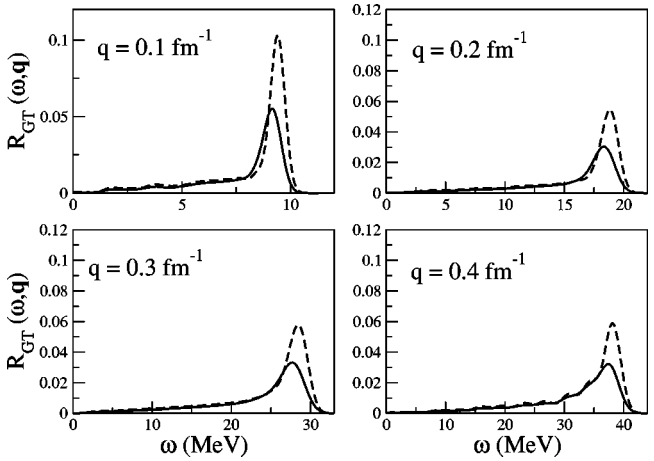

FIG. 13. Gamow-Teller response functions calculated using RPA (solid) and TDA (dashed) with O^{eff}_{GT} and $v^{SK}(m^*)$ for $q=0.1$–0.4 fm^{-1} and $\rho=\rho_0$.

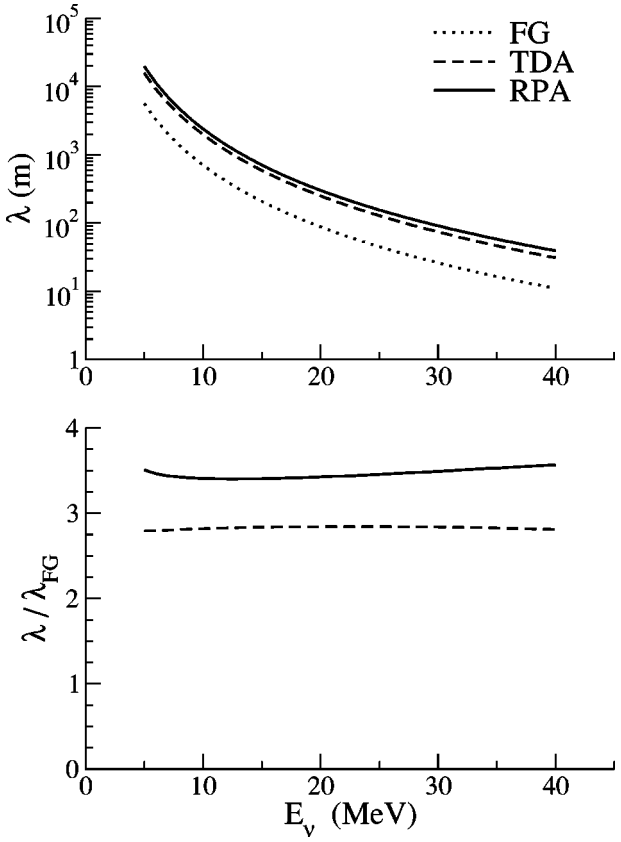

FIG. 14. NMFP for absorption calculated using $v^{SK}(m^*)$ and O^{eff} in RPA (solid), TDA (dashed), and noninteracting FG (dotted) for cold SNM at $\rho=\rho_0$. The lower graph gives the ratio of λ/λ_{FG}.

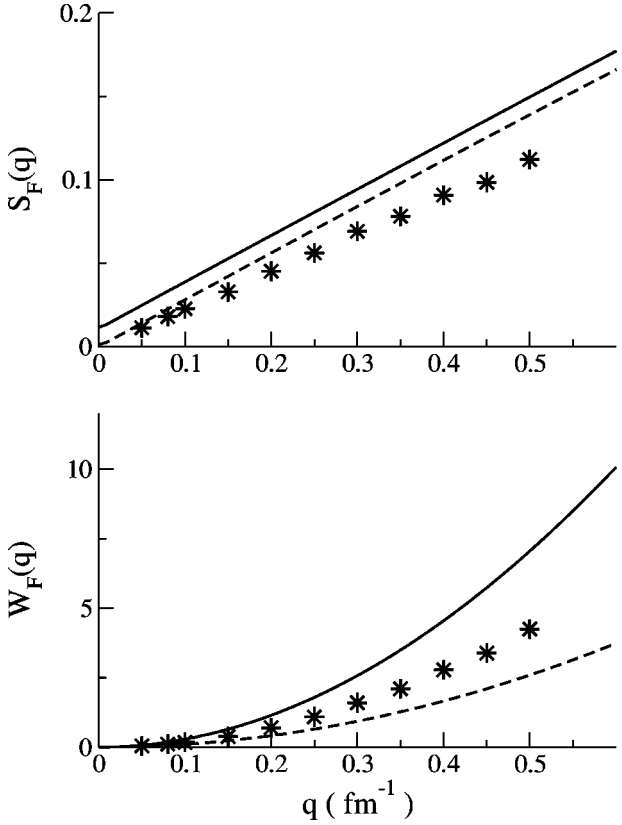

FIG. 15. $S_F(q)$ (upper) and $W_F(q)$ (lower) for the Fermi operator. Results are shown for a noninteracting FG (dashed line), for integrals of the CTDA $R_F(\omega,q)$ (stars) and for the VGS using Eqs. (54) and (56).

$$S(q)=\frac{1}{A}\int\sum_F |\langle\Psi_F|O_W|\Psi_I\rangle|^2\delta(\omega+E_I-E_F)d\omega, \quad (53)$$

$$=\frac{1}{A}\langle\Psi_I|O_W^\dagger O_W|\Psi_I\rangle, \quad (54)$$

and the energy weighted sum

$$W(q)=\frac{1}{A}\int\sum_F |\langle\Psi_F|O_W|\Psi_I\rangle|^2\delta(\omega+E_I-E_F)\omega\, d\omega, \quad (55)$$

$$=\frac{1}{2A}\langle\Psi_I|[O_W^\dagger,[H,O_W]]|\Psi_I\rangle, \quad (56)$$

are calculated using the variational ground state (VGS) obtained in the FHNC-SOC calculations [10,11] and also by direct integration of the CTDA response functions described in Sec. IV. The sums calculated using VGS include both 1*p*-*h* and multi *p*-*h* contributions, while the CTDA with $O^{eff(1b)}$ contains only the contributions of 1*p*-*h* correlated basis states. The multi-*p*-*h* sums are then given by $S_{mph}\approx S^{VGS}-S^{CTDA}$ and $W_{mph}\approx W^{VGS}-W^{CTDA}$.

The static structure function and energy weighted sum for the Fermi response, $S_F(q)$ (upper) and $W_F(q)$ (lower), are shown in Fig. 15. Charge conservation requires $S_F(q=0)=0$. However, $S_F^{VGS}(q)$ (solid line) is nonzero at $q=0$, indicating the error due to approximations in the FHNC-SOC calculation. For the bare weak operators, $S_{bare}^{CTDA}(q)=S^{FG}(q)$ given by the dashed line. $S_F^{CTDA}(q)$ calculated from the CTDA with O^{eff} and shown by the stars is ~20% less than the $S_F^{VGS}(q)$. If we consider $q=0.2$ fm^{-1}, for example, $S_F^{VGS}=0.07$ and $S_F^{CTDA}=0.05$, showing that the 1*p*-*h* contribution to the static structure function is dominant. However the multi-*p*-*h* contribution, $S_{mph}\approx 0.02$, is not negligible.

We can approximate the average energy of the multi-*p*-*h* response using $W_F(q)$. Consider again $q=0.2$ fm^{-1} where $W_F^{VGS}=1.15$ MeV. For the 1*p*-*h* contribution, $W_F^{CTDA}=0.70$ MeV and we find $W_{mph}\approx 0.45$ MeV. The average energy of the multi-*p*-*h* response is

$$E_{mph}\approx\frac{W_{mph}}{S_{mph}}=23\ \text{MeV}, \quad (57)$$

where

$$E_{1ph}\approx\frac{W_F^{CTDA}}{S_F^{CTDA}}=14\ \text{MeV}. \quad (58)$$

Though the contribution of the multi *p*-*h* processes are not negligible, the average energy of the multi *p*-*h* response is much higher than that of the 1*p*-*h* response. The NMFP is most sensitive to the response at low energy transfers where

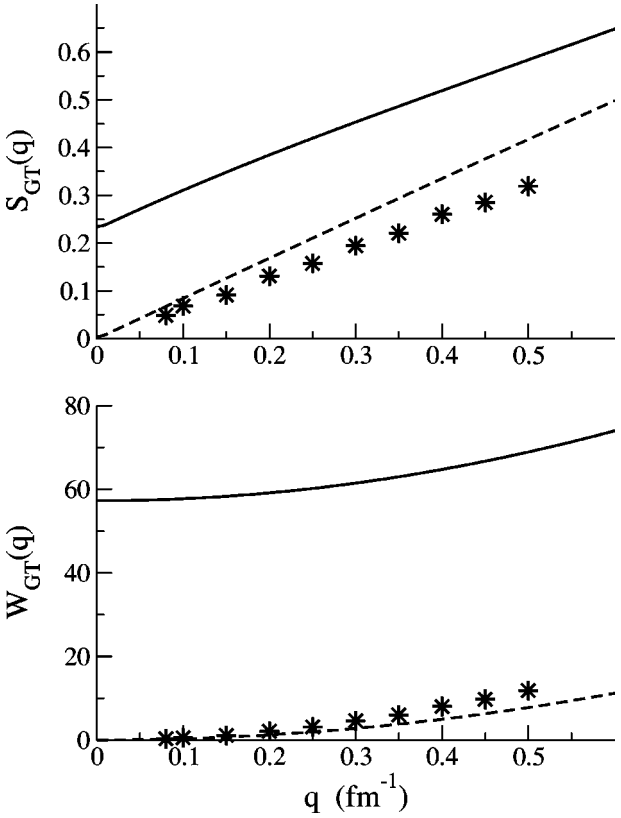

FIG. 16. $S_{GT}(q)$ (upper) and $W_{GT}(q)$ (lower) for the GT operator. See caption of Fig. 15 for notation.

the multi-p-h contribution is not expected to be significant.

Similar results are obtained for the O_{GT} sums shown in Fig. 16. Note that $S_{GT}^{VGS}(q)$ (solid line) is large at $q=0$ as the spin density is not conserved when tensor forces are included. The static structure function again indicates that the multi-p-h contribution is not negligible. However, the average energy of the multi-p-h response is significantly higher than that of the 1p-h response.

It is commonly argued that RPA is the better method for obtaining reaction rates because the energy weighted sums of the response functions satisfy $W^{RPA}(q)=q^2/2m$. This value of the energy weighted sum is correct only when the interaction operator v_{ij} commutes with the perturbation operator $O(q)$. However, the weak operators do not commute with the nuclear forces, and the energy weighted sums calculated using VGS and realistic nuclear forces via Eq. (56) clearly show that $W_F(q)$ and $W_{GT}(q) \gg q^2/2m$ (Figs. 15 and 16).

B. Spin transverse and spin longitudinal sum rules

There are experimental and theoretical indications that the spin longitudinal and spin transverse response functions can differ significantly due to tensor forces. To illustrate this point we calculate the spin longitudinal and spin transverse static structure functions and energy weighted sums for O_{GT} using VGS and by direct integration of the CTDA response functions calculated using O^{eff}. We assume q along the z axis and define the static structure functions as

$$S_L(q) = \frac{1}{A}\int \sum_F |\langle \Psi_F|\hat{q}\cdot O_{GT}|\Psi_I\rangle|^2 \delta(\omega + E_I - E_F) d\omega, \tag{59}$$

$$S_T(q) = \frac{1}{2A}\int \sum_F |\langle \Psi_F|\hat{q}\times O_{GT}|\Psi_I\rangle|^2 \delta(\omega + E_I - E_F) d\omega. \tag{60}$$

For the CTDA, these are simply

$$S_L(q) = \int R_{zz} d\omega, \tag{61}$$

$$S_T(q) = \int R_{xx} d\omega, \tag{62}$$

where the response functions R_{zz} and R_{xx} are defined by Eq. (40).

The energy weighted sums are given by

$$W_L(q) = \frac{1}{A}\int \sum_F |\langle \Psi_F|\hat{q}\cdot O_{GT}|\Psi_I\rangle|^2 \delta(\omega + E_I - E_F)\omega\, d\omega, \tag{63}$$

$$W_T(q) = \frac{1}{2A}\int \sum_F |\langle \Psi_F|\hat{q}\times O_{GT}|\Psi_I\rangle|^2 \delta(\omega + E_I - E_F)\omega\, d\omega. \tag{64}$$

Figures 17 and 18 show the spin longitudinal (upper graph) and spin transverse (lower graph) sums obtained from the VGS (solid line) and CTDA response (stars). We include for reference in Fig. 17, $S_L^{FG}(q)=S_T^{FG}(q)$ calculated for a noninteracting FG (dotted line).

In the longitudinal direction, $S_L^{VGS}(q)$ is significantly larger than the $S_L^{FG}(q)$. It is nonzero at $q=0$ and has a peak value of ~ 1.2 at $q\sim 1.5$ fm^{-1}. However, the 1p-h $S_L^{CTDA}(q)$ is smaller than the FG sum at small q. When $q \gtrsim 0.5$ fm^{-1}, S_L^{CTDA} deviates significantly from the FG sum and more closely matches $S_L^{VGS}(q)$. In this region, the 1p-h contributions are dominant. In principle the sum of the 1p-h response must be smaller than that of the total. The present S_L^{CTDA}, however, exceeds S_L^{VGS} near $q\sim 1.3$ fm^{-1} by $\sim$20%, indicating that the CTDA longitudinal response may be too large.

In the transverse case, $S_T^{VGS}(q)$ differs significantly from the FG sum only at small q, where it is finite at $q=0$. The sum of 1p-h contributions, $S_T^{CTDA}(q)$ is less than both $S_T^{VGS}(q)$ and $S_T^{FG}(q)$ at all values of q.

The energy weighted sums $W_{L,T}^{VGS}$ and $W_{L,T}^{CTDA}$ are shown in Fig. 18. They indicate that the multi-p-h contributions to both longitudinal and transverse responses have larger average energies than the 1p-h contributions.

These sums have been previously calculated using an older variational ground state also obtained with FHNC-SOC methods [10]. The present results do not differ significantly from those previously published for large values of q. However, the range of integration was not long enough in the

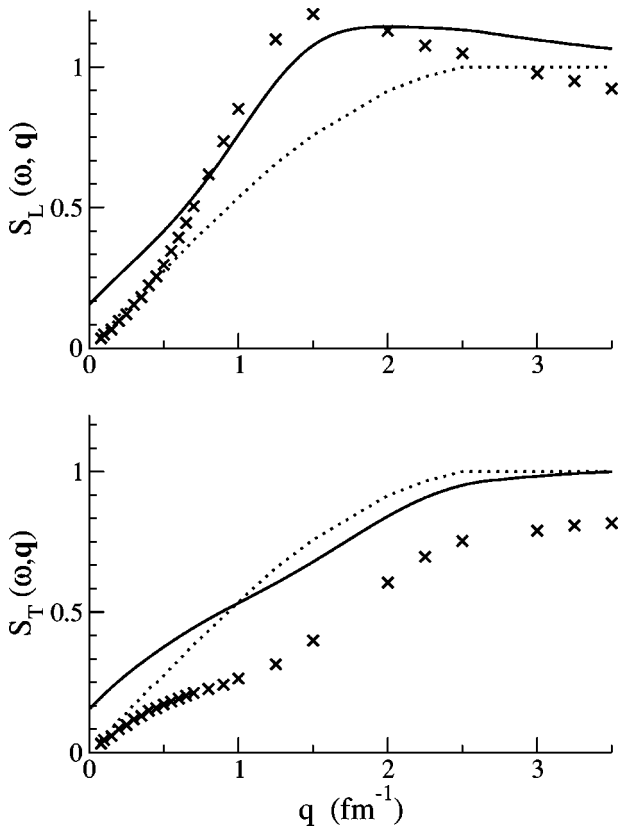

FIG. 17. Spin longitudinal (upper) and spin transverse components of the GT static structure functions calculated using VGS (solid), CTDA (cross marks), and noninteracting FG (dotted).

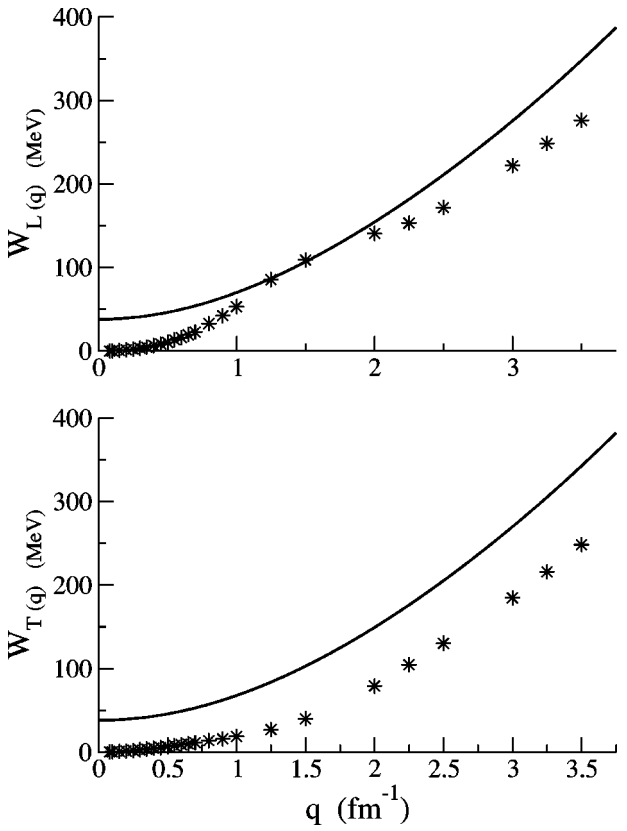

FIG. 18. Spin longitudinal (upper) and spin transverse components of the GT energy weighted sums calculated using VGS (solid) and CTDA (cross marks).

calculations of Ref. [10] to give accurate results at small values of q. At $q \leqslant 0.25$ fm^{-1}, the present calculation is more accurate, and replaces the previous results.

X. CONCLUSIONS

We have calculated the response of cold SNM to weak probes using two-body effective interactions and one-body effective weak operators. These were obtained consistently from realistic nuclear forces using CBT. The infinite system has been modeled using a box with periodic boundary conditions. Using a basis of correlated $1p$-$1h$ excitations, i.e., the correlated TDA, the response for both neutral and charge weak operators have been calculated.

For both charge and neutral weak operators the response is pushed to larger energies when compared to the response of a noninteracting FG. The effective operators suppress the response by 20–25 % relative to calculations using bare operators in most cases. However, for the density or isospin and spin independent term of O_{NV}, the suppression depends sensitively on the density of the system. The effective operator has little effect when $\rho=\rho_0$, but suppresses the "bare" response by $\sim$20% for $\rho=(3/2)\rho_0$.

Using the response functions obtained in CTDA, the NMFP for low energy neutrino scattering and absorption in SNM have been calculated. For neutrino absorption in matter at densities $\rho=\frac{1}{2},1,\frac{3}{2}\rho_0$, λ is enhanced by $\sim$2.5–3.5 relative to λ obtained for a noninteracting FG. Similar results are seen for neutrino scattering at matter densities $\rho=1,(3/2)\rho_0$.

Using the Landau effective mass obtained from the single-particle energy calculated using v^{CBS}, the low energy NMFP can be adequately reproduced using a zero-range Skyrme-like effective interaction, $v^{SK}(m^*)$ and O^{eff}. The $v^{SK}(m^*)$ is chosen to reproduce the spin, isospin and spin-isospin susceptibilities of SNM and the equation of state. Though the responses calculated from v^{CBS} and $v^{SK}(m^*)$ do not agree in detail, the predicted NMFP are nearly the same. Many current approaches use a Skyrme-like effective interaction and bare weak operators. The present calculations indicate that these may overestimate the neutrino cross sections.

We also examine the need to extend the current calculation to include RPA corrections. Using $v^{SK}(m^*)$ the response functions have been calculated using standard RPA methods. For the low energy processes of interest λ_{RPA} for $\rho=\rho_0$ was increased by $\sim$25% relative to λ_{TDA}. The NMFP obtained using v^{CBS} and O^{eff} in RPA including the necessary orthogonality corrections may be $\sim$3 to 4 λ_{FG} in the $1/2$ to $(3/2)\rho_0$ density region.

Though the $1p$-$1h$ response functions calculated here are the dominant contributions to the one-body neutrino processes considered, there are higher-body terms that can contribute via the many-body terms in O^{eff}. The importance of these terms has been estimated using the static structure

function and energy weighted sum. These were calculated using the VGS obtained using FHNC-SOC methods and by direct integration of the CTDA response functions. The sums indicate that though the multi-*p*-*h* response is not negligible, the average energy of their response is much larger than that of the 1*p*-1*h* response. For low energy neutrinos, the NMFP in SNM is dominated by the response at low energy transfers, and the contributions of the multi-*p*-*h* may not be significant.

In the context of supernovae and neutron stars the cold SNM calculations given here are not very useful. However, the present methods can be easily adapted to handle the temperature and proton fraction dependence needed in calculating neutrino rates for modern supernovae and neutron star simulations. In addition, the present cold SNM calculations provide tests of some of the approximations used to study weak interactions in hot asymmetric matter.

ACKNOWLEDGMENTS

This work has been supported in part by the U.S. National Science Foundation via grant PHY-00-98353.

[1] R. Schiavilla and R. B. Wiringa, Phys. Rev. C **65**, 054302 (2002).
[2] A. C. Hayes, P. Navratil, and J. P. Vary, Phys. Rev. Lett. **91**, 012502 (2003).
[3] J. M. Sampaio, K. Langanke, G. Martinez-Pinedo, E. Kolbe and D. J. Dean, Nucl. Phys. **A718**, 440c (2003).
[4] A. Burrows and R. F. Sawyer, Phys. Rev. C **59**, 510 (1999); **59**, 554 (1998).
[5] C. J. Horowitz and M. A. Perez-Garcia, Phys. Rev. C **68**, 025803 (2003).
[6] S. Reddy, M. Prakash, J. M. Lattimer, and J. A. Pons, Phys. Rev. C **59**, 2888 (1999).
[7] N. Iwamoto and C. J. Pethick, Phys. Rev. D **25**, 313 (1982).
[8] A. Arima, K. Shimizu, W. Bentz, and H. Hyuga, Adv. Nucl. Phys. **18**, 1 (1987).
[9] S. Cowell and V. R. Pandharipande, Phys. Rev. C **67**, 035504 (2003).
[10] A. Akmal and V. R. Pandharipande, Phys. Rev. C **56**, 2261 (1997).
[11] J. Morales, V. R. Pandharipande, and D. G. Ravenhall, Phys. Rev. C **66**, 054308 (2002).
[12] S. Fantoni and V. R. Pandharipande, Phys. Rev. C **37**, 1697 (1988).
[13] E. Feenberg, *Theory of Quantum Fluids* (Academic Press, New York, 1969).
[14] S. Fantoni, B. L. Friman, and V. R. Pandharipande, Nucl. Phys. **A399**, 51 (1983).
[15] A. Fabrocini and S. Fantoni, Nucl. Phys. **A503**, 375 (1989).
[16] V. R. Pandharipande and R. B. Wiringa, Rev. Mod. Phys. **51**, 821 (1979).
[17] H. Nakada, Phys. Rev. C **68**, 014316 (2003).
[18] B. Friedman and V. R. Pandharipande, Nucl. Phys. **A361**, 502 (1981).
[19] A. L. Fetter and J. D. Walecka, *Quantum Theory of Many-Particle Systems* (McGraw-Hill, New York, 1971).
[20] T. N. Taddeucci *et al.*, Phys. Rev. Lett. **73**, 3516 (1994).
[21] T. Wakasa *et al.*, Phys. Rev. C **59**, 3177 (1999).
[22] E. Krotscheck, Phys. Rev. A **26**, 3536 (1982).